Smart Structures and Systems, *Vol. 28, No. 5 (2021) 689-698*
https://doi.org/10.12989/sss.2021.28.5.689

Baseline-free damage imaging technique for Lamb wave based structural health monitoring systems

Rahim Gorgin [a] and Ziping Wang*

Faculty of Civil Engineering and Mechanics, Jiangsu University, Zhenjiang 212013, Jiangsu, China

(*Received March 25, 2021, Revised July 15, 2021, Accepted August 6, 20021*)

Abstract. In Lamb wave based structural health monitoring (SHM) systems, damage scatter signals are usually used for damage identification. Such scatters are obtained by subtracting the current signal from a baseline. However, changes in the environmental condition, particularly temperature, make false scatters in the damage scatter signal. This affects the overall efficiently of the system. To overcome this obstacle, this study proposes a baseline-free damage identification technique. A dual-PZT actuation scheme is applied to generate a comparatively pure A_0 mode. A wave velocity determination procedure is then developed to actively determine the velocity of the generated A_0 mode in the presence of unmeasured temperature changes. Using a damage scatter separation process, the damage scatter wave is separated from other waves appear in the current signal. Finally, a damage diagnostic image is constructed to illustrate the most probable location of damage. The experimental validation of the developed technique is conducted on two aluminum plates one carrying an L shape crack and the other carrying a hole, subjected to temperatures changes. The experimental results demonstrate the effectiveness of the developed technique for damage identification in the presence of unmeasured temperature. During the proposed procedure no baseline data is used. This bright advantage, qualify the presented technique for practical SHM systems.

Keywords: damage imaging technique; lamb wave; piezoelectric transducer; structural health monitoring

1. Introduction

Most of industrial equipment utilized in mechanical, civil, and aerospace applications, serve at harsh conditions. Hence, they are prone to many types of damages such as cracks and corrosion in metallic structures and delamination in composite laminates.

Since damages are a real threat for the reliability of a structure, a considerable amount of study has been conducted in order to identify the location and size of damages in structures.

Structural health monitoring (SHM) is a technology with smart algorithms to assess the 'health' status of structures in real time (Wan *et al*. 2021, Gorgin 2020, Wan and Ni 2019, Zheng *et al*. 2019, Mori *et al*. 2019, He *et al*. 2019, Zhou *et al*. 2019, Wan and Ni 2018, Gorgin *et al*. 2015). Toward this topic, Lamb waves, have been increasingly utilized to develop several SHM techniques (Wu *et al*. 2009, Gorgin *et al*. 2014, Gao *et al*. 2018, Wang *et al*. 2018a, b, Qing *et al*. 2019).

Since Lamb waves travel long distances in the structure and can be generated and collected with piezoelectric transducers (PZT) that require little power, they are appropriate for structural health monitoring systems (Kudela *et al*. 2018, Muller *et al*. 2019).

When Lamb wave is incident on damage, it scatters in all directions. These scatter waves can be used to identify and characterize the damage. Usually, damage scatter waves are obtained by subtracting the current signal from a baseline. However, there are certain drawbacks in using baseline signal.

Firstly, baseline signal might not be available. Secondly, environmental and operational conditions (EOCs) variation (particularly temperature) can change the velocity and amplitude of the current signal even in absence of any damage (Gorgin *et al*. 2020). This has a negative effect on the active SHM system. To overcome these limitations, many researchers have proposed baseline free damage detection techniques.

Time reversibility of Lamb wave is widely used for baseline free damage detection techniques (Park *et al*. 2009, Poddar *et al*. 2011, Bijudas *et al*. 2013). A modified time reversal method in which the frequency dependence of the time reversal operator is compensated, is proposed by Zeng *et al*. (2017). An enhanced Lamb wave virtual time reversal (VTR) method with transducer transfer function compensation to omit the transducer effect for dispersive, multimodal Lamb waves is presented by Wang and Shen (2019). Some probabilistic diagnostic imaging technique using time reversal approach were also presented in references (Miao *et al*. 2011, Zhu *et al*. 2013). In addition to time reversal approach, some other baseline free damage detection techniques have been proposed by researchers. Park *et al*. (2010) have presented the concept of transfer impedance of PZT transducers for baseline free damage detection. A method based on identifying the first arrival of

*Corresponding author, Ph.D.,
E-mail: wzp@ujs.edu.cn
[a] Ph.D.

ISSN: 1738-1584 (Print), 1738-1991 (Online)

A_0 mode from a delamination in the path of wave propagation is proposed by Yeum *et al*. (2014). Alem *et al*. (2016) have developed a baseline free method based on cross-correlation analysis. Alguri *et al*. (2018) have proposed a dictionary learning framework. This method combines wave propagation characteristics of a host structure with geometric information of surrogate structures to develop a baseline free damage detection method. In another study, a baseline free method using a dual PZT network is developed by Lizé *et al*. (2018). Another method based on reciprocity principle is presented by Huang *et al*. (2017). Recently, a method which make use of a distance compensation algorithm for pitch-catch pairs of different length, is proposed by Qiu *et al*. (2019). Another baseline free method using a time-space analysis is presented by Li and Chattopadhyay (2019).

In this study, a baseline-free damage imaging technique is developed. In order to generate a comparatively pure A_0 mode, a dual-PZT actuation scheme is applied. Since, temperature variation, changes the velocity of the current signal, a wave velocity determination procedure is developed to actively determine the velocity of the A_0 mode without any interpretation of the current signal. Then, a damage scatter separation process is presented to separate the damage scatter wave from other waves appear in the current signal, using the obtained A_0 mode velocity. Finally, a diagnostic image is constructed to show the most probable location of damage in the structure. This procedure is applied to experimental data from two aluminum plates one carrying an L shape crack and the other carrying a hole, subjected to temperatures variations in a controlled thermal environment.

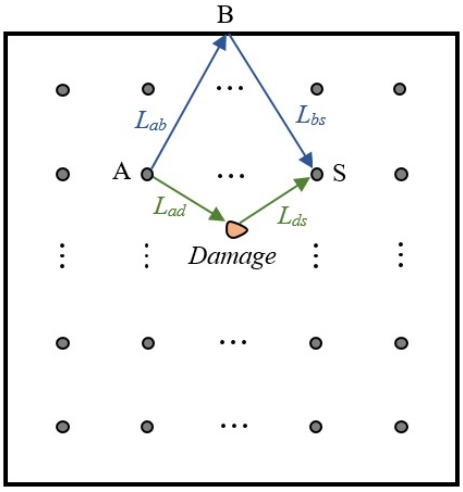

Fig. 1 A sparse sensor network consisting N transducer

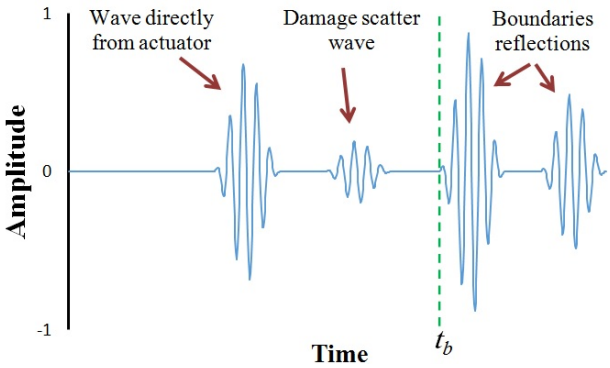

Fig. 2 Typical Lamb wave signal

2. Baseline-free damage imaging technique

The presented baseline-free damage imaging technique consists of three steps including the A_0 mode velocity determination procedure, damage scatter separation process, and damage diagnostic image construction.

2.1 The A_0 mode velocity determination procedure

Temperature affects the material properties of the structure and piezoelectric transducers, causing changes in Lamb wave propagation properties such as wave velocity. Hence, in this section, a procedure is presented to determine the A_0 mode velocity of current signal.

Consider a sparse sensor network, with N transducer in conformity to the pitch-catch $\left(A_i - S_j(i,j = 1,2,\dots,N,)\right.$ but $\left.i \neq j\right)$ configuration to generate and acquire Lamb wave signals into the structure as is shown in Fig. 1. L_{ad} and L_{ds} are the direct distances between the damage and respectively actuator and sensor.

Captured Lamb wave signals consist of three components in time domain including the wave which directly comes from the actuator, the probable damage scatter wave and the reflections from structure boundaries as shown in Fig. 2.

The direct distance between the actuator and sensor is shorter than the distance from the actuator to damage and then from damage to sensor. Also, it is shorter than the distance from actuator to the boundary and then from boundary to sensor. Hence, the first wave which appears in the current signal is the A_0 mode.

In order to determine the velocity of the A_0 mode, the direct distance between the actuator to the sensor should be divided by the time in which the wave travels from the actuator to the sensor.

This time is usually defined as the time between the energy envelope peak of the excitation signal and the energy envelope peak of the separated signal. Since, in some cases, due to the interactions of the boundaries reflections, their amplitudes may be higher than the amplitude of the A_0 mode which directly comes from the actuator, determining the time in which the wave travels from the actuator to the sensor, in this way and without the interpretation of the signal may leads to false results.

This limits the application of the damage identification technique for real-time structural health monitoring systems. To tackle this deficiency, the boundaries reflections need to be eliminated from the collected signal. As can be seen in Fig. 2, the primarily beginning time of the boundaries reflections (t_b) can be defined as follow

$$t_b = \frac{L_{ab} + L_{bs}}{v} \tag{1}$$

Where, L_{ab} and L_{bs} are direct distances between the point B and respectively actuator and sensor (see Fig. 1). Point B, is a point in the boundaries of the structure which gives the minimum amount of $L_{ab}+L_{bs}$. v is the A_0 mode velocity.

However, in practice, due to the lack of information about the operational temperature of the structure the A_0 mode velocity is also indefinite. Therefore, first we assume that the structure is serving at its minimum operational temperature. By decreasing temperature, the wave velocity increases. Therefore, at minimum operational temperature, the A_0 mode velocity is maximum. While there is the possibility of mode conversion for the reflected waves, using the maximum wave velocity in Eq. (1) ensures that all the boundaries reflections will be eliminated from the collected signal.

Now, in the time period $[0, t_b]$, the collected signal only includes the A_0 mode that directly comes from the actuator and the possible damage scatter wave. Then, the energy envelope of the separated signal can be obtained as follow

$$e(t)=\sqrt{s^2(t)+H^2(t)} \tag{2}$$

Where, $e(t)$ is the energy envelope of the separated signal, $s(t)$ is the separated signal and $H(t)$ is the Hilbert transform of the separated signal and defined as

$$H(t)=\frac{1}{\pi}\int_{-\infty}^{+\infty}\frac{s(t')}{t-t'}dt' \tag{3}$$

As is shown in Fig. 3, the time (t_{as}) that wave travels from the actuator to the sensor can be easily defined as the time between the energy envelope peak of the excitation signal and the energy envelope peak of the separated signal.

Finally, using t_{as} and the linear distance from the actuator to the sensor (d_{as}), the exact A_0 mode velocity (v_c) in the presence of unmeasured temperature changes can be defined as follow

$$v_c=\frac{d_{as}}{t_{as}} \tag{4}$$

Since, the procedure does not require any interpretation of the current signal, it is suitable for actively determination of Lamb wave velocity in SHM systems.

2.2 Damage scatter separation process (DSSP)

By substituting the accurate velocity of the A_0 mode, in Eq. (1), the accurate beginning time of the boundaries reflections can be determined as follow

$$t_{ab}=\frac{L_{ab}+L_{bs}}{v_c} \tag{5}$$

Where t_{ab} is the accurate beginning time of the boundaries reflections. Using this time, Thus, the wave which directly comes from the actuator and the probable damage scatter wave are separated from the boundaries reflections.

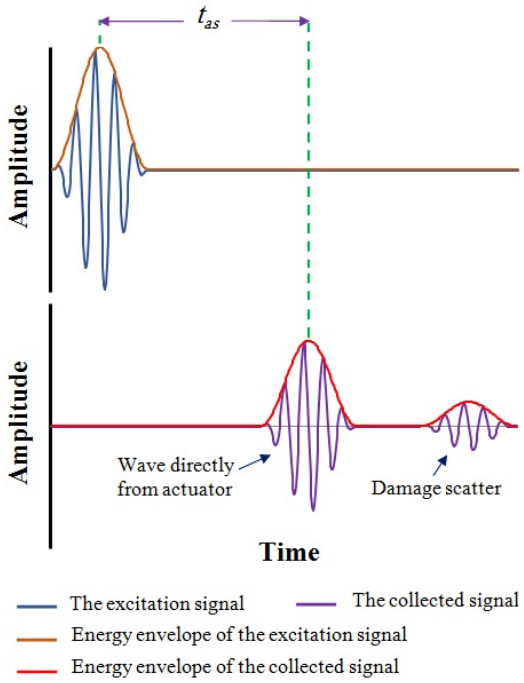

Fig. 3 Typical excitation signal and the separated signal

However, still the probable damage scatter wave must be separated from the wave which directly comes from the actuator.

As can be seen in Fig. 2, the first wave that appears in the acquired signal is the wave which directly comes from the actuator.

Therefore, based on the linear distance between the actuator to the sensor, the A_0 mode velocity and the length of the excitation signal, the ending time of the wave which directly comes from the actuator can be determined as follow

$$t_{ad}=\frac{L_{as}}{v_c}+L \tag{6}$$

Where, t_{ad} is the ending time of the wave which directly comes from the actuator, L_{as} is the linear distance between the actuator and the sensor, and L is the length of the excitation signal.

Using this time, the probable damage scatter can be separated from the wave which directly comes from the actuator.

Generally, based on Eqs. (5) and (6), a rectangular window function can be used to define the scatter signal. Its expression is

$$f=\begin{cases}0 & 0\le t<t_{ad}\\ 1 & t_{ad}\le t<t_{ab},\ t_{ad}=\dfrac{L_{as}}{v_c}+L,\\ 0 & t\ge t_{ab}\end{cases} \quad \text{and}\ \ t_{ab}=\frac{L_{ab}+L_{bs}}{v_c} \tag{7}$$

When the collected signal be multiplied by this function, the damage scatter wave will be separated from other waves.

2.3 Diagnostic image construction

Assume that the data acquisition process has been done in N locations of the monitoring area. The A_0 mode velocity is determined and the damage scatter signal corresponds to each response has been obtained by using the damage scatter separation process.

The monitoring area is meshed with $K \times L$ uniformly distributed grids. An image can be constructed by relating the contrast at a grid point to the amplitude of the damage scatter signal. However, since the damage scatter wave has five cycles in the time domain, the imaging result will be speckled which results in difficulty to identify the exact location of damage.

To tackle this problem, the energy envelope of the damage scatter signal is utilized instead of the amplitude of the damage scatter signal. The energy envelope of the signal is equivalent to its outline and an envelope detector connects all the peaks in this signal.

For each damage scatter signal, a probability image can then be constructed as follow

$$I_n(i,j) = e_n\left(t_{nij}\right), \quad n = 1,2,\ldots,N \text{ and } t_{nij} = \frac{L_n^{ad} + L_n^{ds}}{v_c} \tag{8}$$

Where, $I_n(i,j)$ represents the probability of damage presence in the imaging grid point (i,j), $e_n(t)$ is the energy envelope of the damage scatter signal correspond to signal acquired at location n, and t_{nij} is the time in which wave travels from actuator to the imaging grid point (i,j) and then from the imaging grid point (i,j) to the sensor. L_n^{ad} denotes the linear distance between actuator at location n and the imaging grid point (i,j) and L_n^{ds} is the linear distance between the imaging grid point (i,j) and the sensor at location n. v_c is the current A_0 mode velocity.

Probability images highlight the points which have the highest probability of damage presence in the structure. The diagnostic image can finally be constructed by adding all I_n determined from different responses such that

$$P(i,j) = \sum_{n=1}^{N} I_n(i,j) \tag{9}$$

Where, $P(i,j)$ represents damage presence probability in grid point (i,j).

The imaging grid points with the maximum values demonstrate the probable location of damages in the structure.

3. Experimental setup

The presented baseline-free damage detection technique was used to determine the location of an L shape crack and a hole in two same size aluminium plates at different temperatures. The dimension of the plates was chosen equal to 400 mm × 400 mm × 3 mm due to the limitation in the available space of the climate chamber.

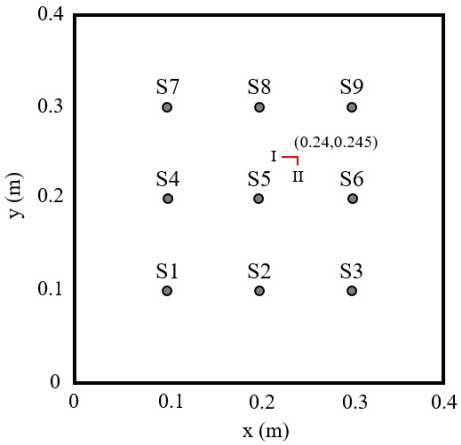

Fig. 4 An aluminum plate with an L shape crack

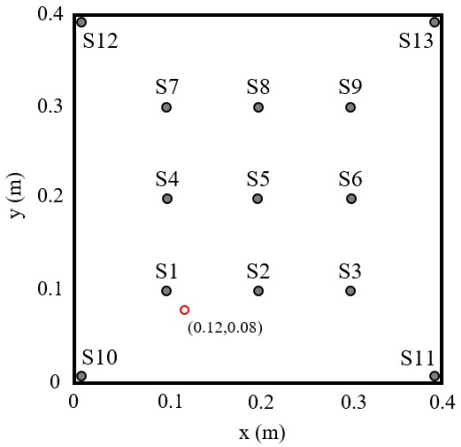

Fig. 5 An aluminum plate with a hole

On the plate with an L shape crack, a sparse sensor network with pitch-catch configuration was set up with 9 pairs of PZT transducers (APC 851). On the plate with a hole, a sparse sensor network was set up with 13 pairs of PZT transducers (APC 851). A dual-PZT actuation scheme was applied to generate a comparatively pure A_0 mode with enhance energy.

The L shape crack consisted of two through-thickness edges (edge I and II, respectively being 15 and 5 mm long and both have 0.2 mm wide), as is demonstrated in Fig. 4 and the hole has 15 mm diameter as is shown in Fig. 5.

The aluminium plates were placed into a climate chamber device called as ESPEC, where the temperature can change from the room temperature to 250°C. The minimum operational temperature of the plate was considered equal to the room temperature (20°C).

Lamb wave generation and collection were done using Scan Genie machine. Piezoelectric transducers were acted as both actuator and sensor with the aid of a two-way switch.

A 5-cycle sinusoidal toneburst enclosed in a Hanning window with the length of 0.1 ms was generated and collected at a sampling rate of 48 MHz. Since due to the mode tuning effect, at lower frequencies the fundamental antisymmetric wave mode has a higher relative amplitude

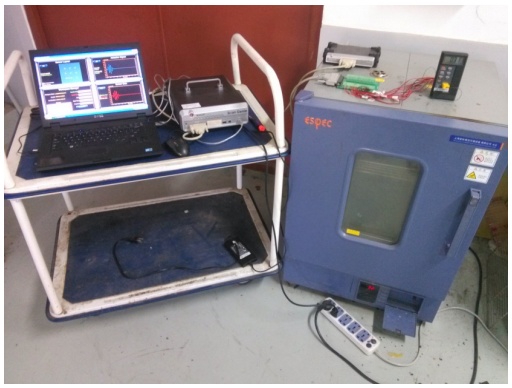

Fig. 6 Experimental setup

compared to the fundamental symmetric wave mode (Giurgiutiu 2005), the frequency of the excitation was set to 50 kHz to enhance the energy of the A_0 mode.

Temperature was increased from room temperature $20^{\circ}C$ to $60^{\circ}C$ (five stages in total) in $10^{\circ}C$ increment in each stage. At each stage, for all sensing paths (totally 72) the Lamb wave signals were collected. Experimental setup is shown in Fig. 6.

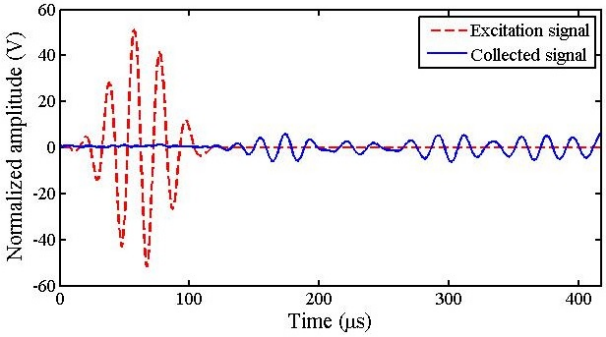

Fig. 7 The excitation signal and a typical response collected by sensor network at 20°C

4. Results and discussion

Firstly, the tests were conducted on the plate with an L shape crack. The signals which were collected at room temperature (20°C), were utilized to evaluate the effectiveness of the developed technique in highlighting damage in the monitoring area. The excitation signal and the typical response collected by sensor network at 20°C, are demonstrated in Fig. 7.

In 20°C which was considered as the minimum operational temperature of the plate, the theoretical value of the A_0 mode velocity in an aluminium plate with 3 mm thickness at 50 KHz is 2203.2 m/s. This velocity is used as the first assumption in the current A_0 mode velocity determination process. The current A_0 mode velocity was determined equal to 2198 m/s, which is very close to the theoretical value. This is exactly what was expected because the current temperature of the plate was 20°C.

By using the damage scatter separation process, the damage scatter signals of all sensing paths were obtained. Since, after damage scatter separation process, some parts of the collected signal are eliminated, each sensing path can only cover some points of the structure under inspection. In fact, each sensing path can highlight those damages where their $(L_{ad} + L_{ds})$ be less than $(L_{ab} + L_{bs})$. For example, Fig. 8(a) demonstrates the points which can be covered by sensing path 2-6.

In all these points $L_{ad} + L_{ds} < L_{ab} + L_{bs}$. Similarly, Fig. 8(b) demonstrates the points which can be covered by sensing path 7-2. If damage be in this area, the damage scatter signal of sensing path 7-2 will contain this damage's scatters, otherwise the damage scatter signal will be zero.

For each sensing path a probability image was constructed. Fig. 9, demonstrates two typical probability images constructed based on the sensing paths 2-6 and 7-2. As can be seen in Fig. 9, the probability image of each sensing path highlights an elliptical set of points including the actual location of damage, which have the maximum probability of damage location. If a sensing path, does not cover the actual location of damage, it constructs

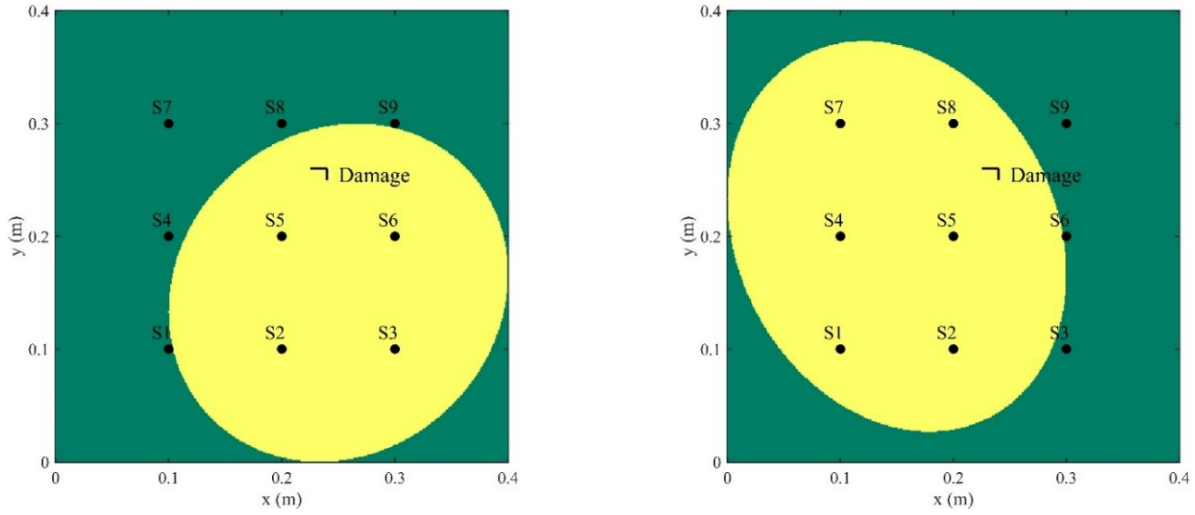

(a) (b)

Fig. 8 The area (in yellow) that can be covered by sensing paths (a) 2-6; (b) 7-2

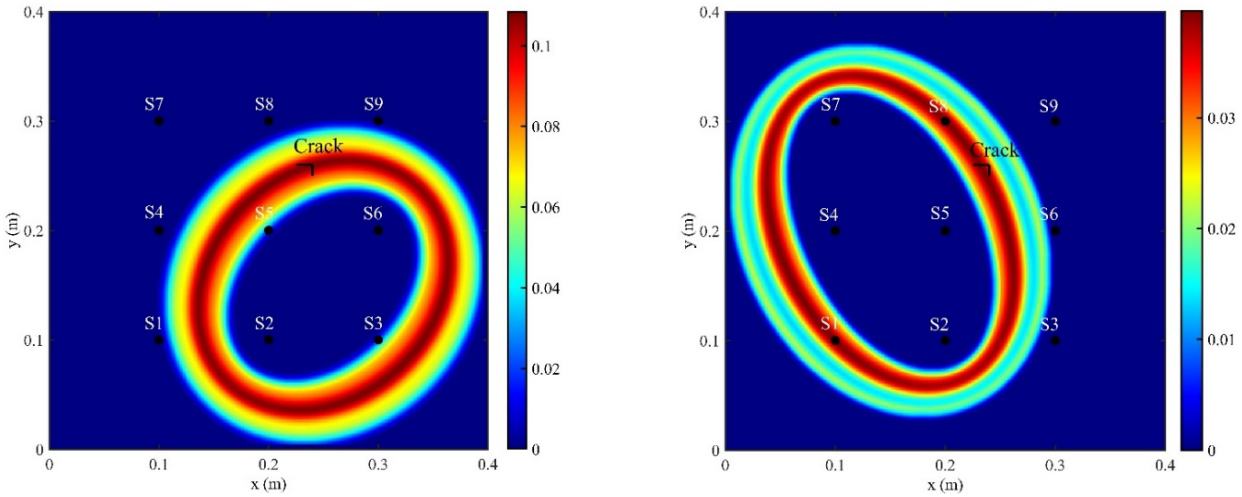

(a) (b)

Fig. 9 Typical probability images constructed by sensing paths (a) 2-6; (b) 7-2

a probability image which the probability value in all points is zero.

The diagnostic image which is constructed by adding all probability values determined from different sensing paths, can highlight those damages which are covered by at least three sensing paths.

In other words, the intersection of at least three elliptical set of points with the maximum probability of damage location is required in order to highlight the exact location of damage. Therefore, the diagnostic image can only highlight those damages where located at points which can be covered by at least three sensing paths. Such points for this set of sensor network are shown in Fig. 10.

As can be seen in Fig. 10, this set of sensor network is not able to cover those points at the corners of the plate. To overcome this deficiency, four pairs of sensor are added at the corners of the plate with a hole (see Fig. 5). In this way, in each sensing path with one of these four pair of sensors, the direct wave and the first boundary reflections are received at the same time and will be deleted in damage

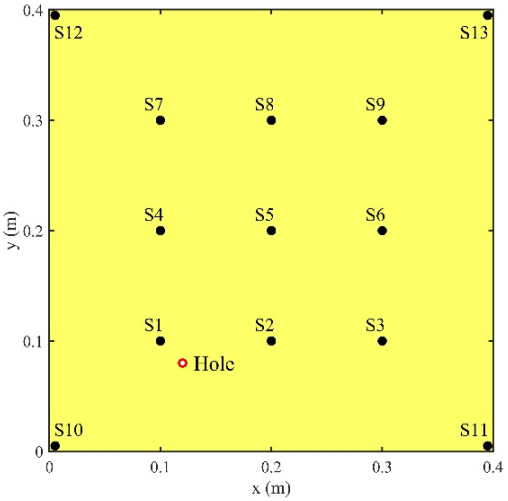

Fig. 11 The area (in yellow) which can be covered by at least three sensing paths of the optimized sensor network

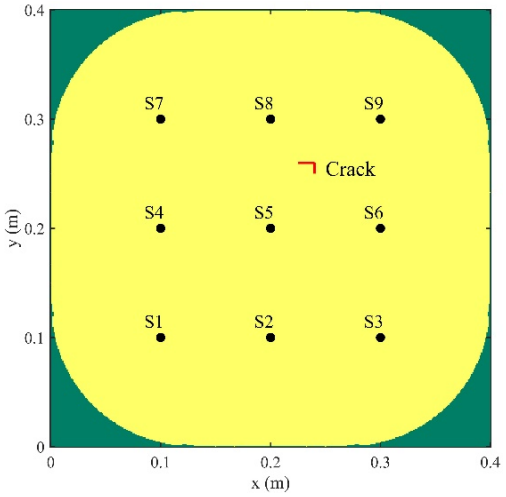

Fig. 10 The area (in yellow) which can be covered by at least three sensing paths

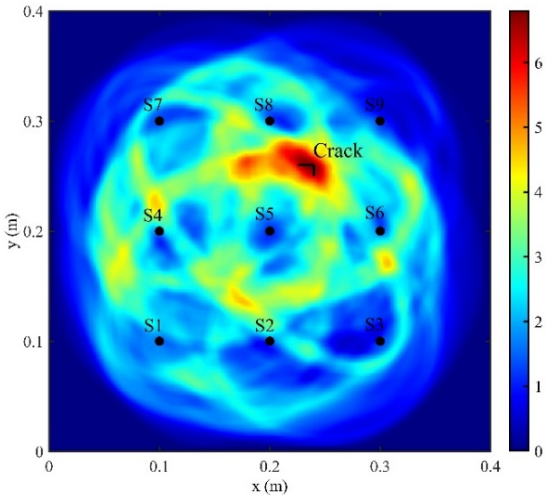

Fig. 12 The damage diagnostic image constructed based on signals collected at 20°C

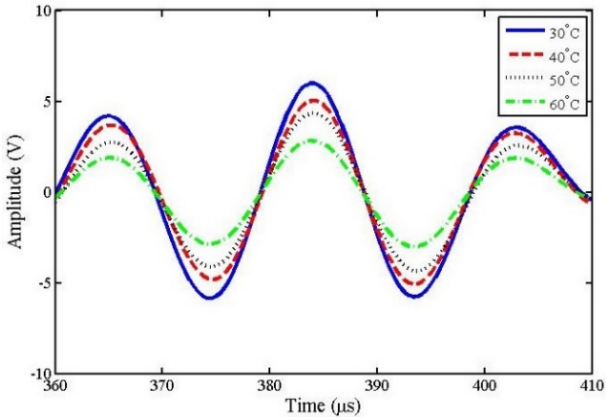

Fig. 13 A part of the collected signals by sensing path 1-9, at different temperatures

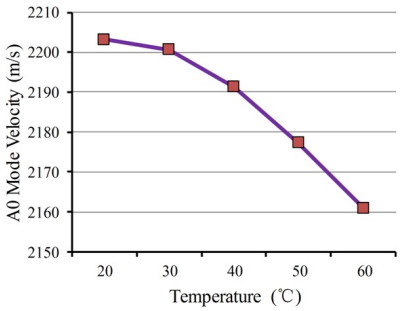

Fig. 14 The A_0 mode velocity defined at different

scatter separation process.

It should be mentioned that in the damage scatter separation of such sensing paths, t_{ab} is the time in which the second boundary reflection is sensed by the sensor. As is shown in Fig. 11, the whole plate can be covered by such an optimized sensor network.

The damage diagnostic image was then constructed for the plate with an L shape crack, by adding all probability values obtained by different sensing paths. In order to enhance the quality of the damage diagnostic image, an average process is utilized.

To do this, the new value of each grid point is the average of the nearest 81 grid points values. Fig. 12 demonstrates the final damage diagnostic image constructed based on signals collected at 20°C.

As can be seen in Fig. 12, the grid points with the highest probability of damage presence, coincide well with the actual location of the introduced crack which demonstrates the effectiveness of the developed technique

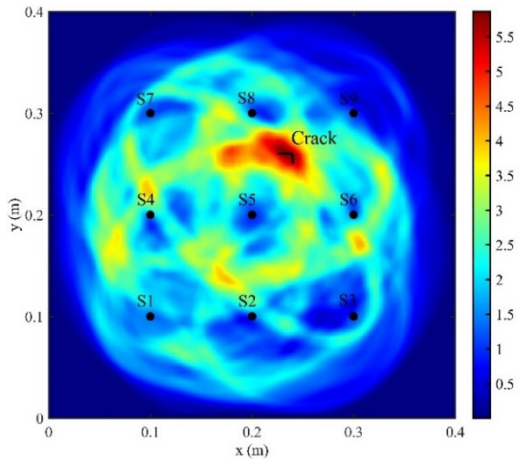

(a) At 30°C

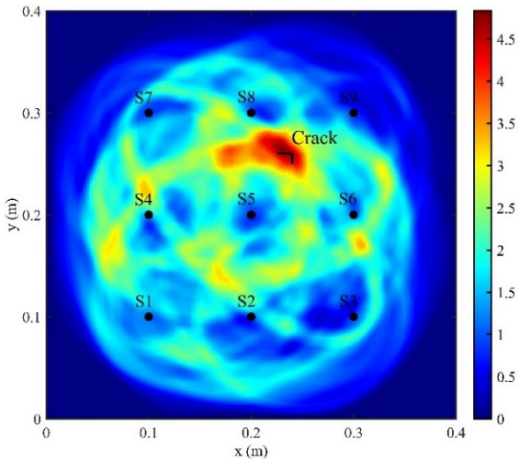

(b) At 40°C

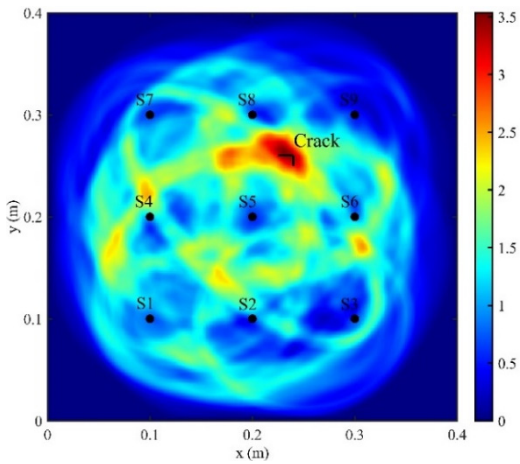

(c) At 50°C

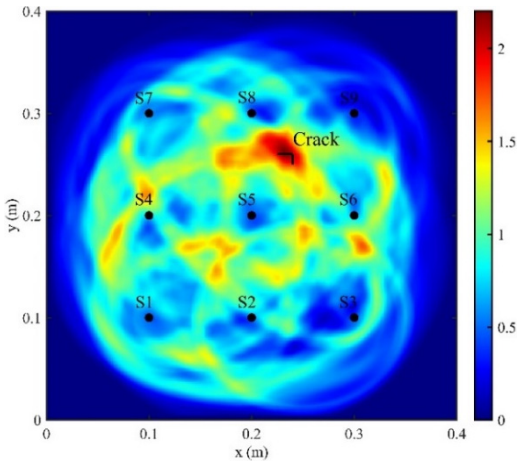

(d) At 60°C

Fig. 15 The damage diagnostic images constructed at different temperatures

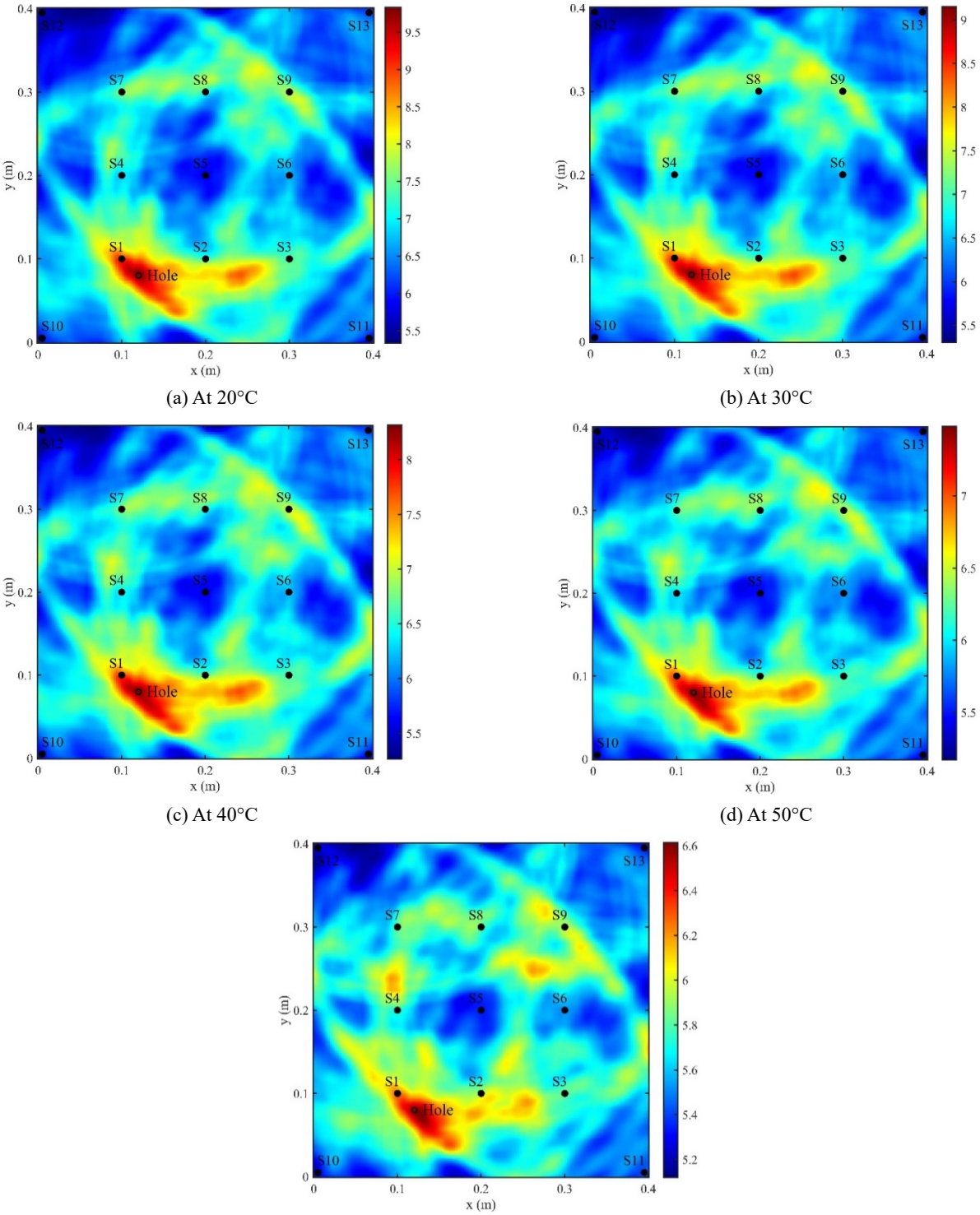

(a) At 20°C

(b) At 30°C

(c) At 40°C

(d) At 50°C

(e) At 60°C

Fig. 16 The damage diagnostic images constructed at different temperatures for aluminum plate with optimized sensor network and a hole

in highlighting damage without using any baseline data.

Fig. 13 displays a part of the collected signals by sensing path 1-9, at different temperatures.

As is shown in Fig. 13, by increasing temperature, the amplitude of the collected signal decreases and the waves are shifted to the right which indicates a decline in the A_0 mode velocity.

The A_0 mode velocity at 20°C (2203.2 m/s) was chosen as the first assumption in the current A_0 mode velocity determination process and the actual A_0 mode velocities at different temperatures were determined and are shown in Fig. 14.

Subsequently, using the damage scatter separation process, the damage scatter signals of all sensing paths at

different temperatures were obtained and the damage diagnostic images were constructed. Fig. 15 demonstrates the damage diagnostic images constructed at different temperatures.

As can be seen in Fig. 15, at different temperatures, the grid points with the maximum probability of damage presence coincide well with the actual location of the introduced crack. This demonstrates the effectiveness of the developed technique in highlighting damages in the structure in the presence of unmeasured temperature.

Moreover, by increasing temperature, the damage presence probability values are decreased. This is because of the decrease in the amplitude of the signal by increasing temperature.

Nevertheless, the diagnostic images do not have a significant change. Since the goal of the presented method is damage localization, what is actually important is to highlight the grid points with the maximum probability values and the maximum probability value itself is not important.

In order to check the performance of the developed method in highlighting damages at different locations of the structure, the procedure was repeated for the plate with a hole. Signals were acquired at 20°C, 30°C, 40°C, 50°C and 60°C and the damage diagnostic images were constructed and are shown in Fig. 16.

As can be seen in Fig. 16, in all temperatures, the grid points with the maximum probability of damage presence coincide well with the actual location of the introduced hole. This demonstrates the effectiveness of the developed technique in highlighting different types of damage, in different locations of the structure, in the presence of unmeasured temperature.

5. Conclusions

In this paper, a baseline-free damage identification method is proposed for temperature compensation in Lamb wave based SHM systems. The presented technique was consisted of three steps. Firstly, the velocity of the current A_0 mode was determined in the presence of unmeasured temperature. Then, damage scatter wave was separated from other waves appear in the collected signal. Finally, based on the energy envelope of the damage scatter signals a damage diagnostic image was constructed which intuitively highlights the most probable location of damages in the structure. Satisfactory experimental results for the identification of an L shape crack and a hole in aluminum plates, subjected to different temperatures, demonstrated that the proposed method is capable to normal temperature range.

During the proposed procedure no baseline data was used. Moreover, the developed technique didn't need any interpretation of the signals. These bright advantages, qualify the presented technique for practical active SHM systems.

References

Alem, B., Abedian, A. and Nasrollahi-Nasab, K. (2016), "Reference-free damage identification in plate-like structures using Lamb-wave propagation with embedded piezoelectric sensors", *J. Aerosp. Eng.*, **29**(6). https://doi.org/10.1061/(ASCE)AS.1943-5525.0000646

Alguri, K.S., Melville, J. and Harley, J.B. (2018), "Baseline-free guided wave damage detection with surrogate data and dictionary learning", *J. Acoust. Soc. Am.*, **143**(6), 3807. https://doi.org/10.1121/1.5042240

Bijudas, C.R., Mitra, M. and Mujumdar, P.M. (2013), "Time reversed Lamb wave for damage detection in a stiffened aluminum plate", *Smart Mater. Struct.*, **22**(10), 105026. https://doi.org/10.1088/0964-1726/22/10/105026

Gao, D., Wu, Z., Yang, L. and Zheng, Y. (2018), "Integrated impedance and Lamb wave–based structural health monitoring strategy for long-term cycle-loaded composite structure", *Struct. Health Monitor.*, **17**(4), 763-776. https://doi.org/10.1177/1475921717717312

Giurgiutiu, V. (2005), "Tuned Lamb Wave Excitation and Detection with Piezoelectric Wafer Active Sensors for Structural Health Monitoring", *J. Intell. Mater. Syst. Struct.*, **16**(4), 291-305. https://doi.org/10.1177/1045389X05050106

Gorgin, R. (2020), "Damage identification technique based on mode shape analysis of beam structures", *Structures*, **27**, 2300-2308. https://doi.org/10.1016/j.istruc.2020.08.034

Gorgin, R., Wu, Z., Gao, D. and Wang, Y. (2014), "Damage size characterization algorithm for active structural health monitoring using the A0 mode of Lamb wave", *Smart Mater. Struct.*, **23**(3), 035015. https://doi.org/10.1088/0964-1726/23/3/035015

Gorgin, R., Ma, Y., Wu, Z., Gao, D. and Wang, Y. (2015), "Probabilistic-based damage identification based on error functions with an autofocusing feature", *Smart Struct. Syst., Int. J.*, **15**(4), 1121-1137. https://doi.org/10.12989/sss.2015.15.4.1121

Gorgin, R., Luo, Y. and Wu, Z. (2020), "Environmental and operational conditions effects on Lamb wave based structural health monitoring systems: A review", *Ultrasonics*, **105**, 106114. https://doi.org/10.1016/j.ultras.2020.106114

He, J., Rocha, D.C., Leser, P.E., Sava, P. and Leser, W.P. (2019), "Least-squares reverse time migration (LSRTM) for damage imaging using Lamb waves", *Smart Mater. Struct.*, **28**(6), 065010. https://doi.org/10.1088/1361-665X/ab14b1

Huang, L., Zeng, L. and Lin, J. (2017), "Baseline-free damage detection in composite plates based on the reciprocity principle", *Smart Mater. Struct.*, **27**(1), 015026. https://doi.org/10.1088/1361-665X/aa9cc1

Kudela, P., Radzienski, M., Ostachowicz, W. and Yang, Z. (2018), "Structural health monitoring system based on a concept of Lamb wave focusing by the piezoelectric array", *Mech. Syst. Signal Process.*, **108**, 21-32. https://doi.org/10.1016/j.ymssp.2018.02.008

Li, G. and Chattopadhyay, A. (2019), "Reference-free damage localization in time-space domain for structural health monitoring of X-COR sandwich composites", *J. Intell. Mater. Syst. Struct.*, **30**(3), 371-385. https://doi.org/10.1177/1045389X18810803

Lizé, E., Rébillat, M., Mechbal, N. and Bolzmacher, C. (2018), "Optimal dual-PZT sizing and network design for baseline-free SHM of complex anisotropic composite structures", *Smart Mater. Struct.*, **27**(11), 115018. https://doi.org/10.1088/1361-665X/aad534

Miao, X., Wang, D., Ye, L., Lu, Y., Li, F. and Meng, G. (2011), "Identification of dual notches based on time-reversal Lamb waves and a damage diagnostic imaging algorithm", *J. Intell.*

Mater. *Syst*. *Struct*., **22**(17), 1983-1992. https://doi.org/10.1177/1045389X11421821

Mori, N., Biwa, S. and Kusaka, T. (2019), "Damage localization method for plates based on the time reversal of the mode-converted Lamb waves", *Ultrasonics*, **91**, 19-29. https://doi.org/10.1016/j.ultras.2018.07.007

Muller, A., Soutis, C. and Gresil, M. (2019), "Image reconstruction and characterisation of defects in a carbon fibre/epoxy composite monitored with guided waves", *Smart Mater*. *Struct*., **28**(6), 065001. https://doi.org/10.1088/1361-665X/ab1359

Park, H.W., Kim, B. and Sohn, H. (2009), "Understanding a time reversal process in Lamb wave propagation", *Wave Motion*, **46**(7), 451-467. https://doi.org/10.1016/j.wavemoti.2009.04.004

Park, S., Lee, C. and Sohn, H. (2010), "Reference-free crack detection using transfer impedances", *J*. *Sound Vib*., **329**(12), 2337-2348. https://doi.org/10.1016/j.jsv.2009.04.010

Poddar, B., Kumar, A., Mitra, M. and Mujumdar, P.M. (2011), "Time reversibility of a Lamb wave for damage detection in a metallic plate", *Smart Mater*. *Struct*., **20**(2), 025001. https://doi.org/10.1088/0964-1726/20/2/025001

Qing, X., Li, W., Wang, Y. and Sun, H. (2019), "Piezoelectric transducer-based structural health monitoring for aircraft applications", *Sensors*, **19**(3), 545. https://doi.org/10.3390/s19030545

Qiu, J., Li, F., Abbas, S. and Zhu, Y. (2019), "A baseline-free damage detection approach based on distance compensation of guided waves", *J*. *Low Freq*. *Noise Vib*. *Active Control*, **38**(3-4), 1132-1148. https://doi.org/10.1177/1461348418813699

Wan, H-P., Dong, G-S. and Luo, Y. (2021), "Compressing sensing of wind speed data of large-scale spatial structures with dedicated dictionary using time-shift strategy", *Mech*. *Syst*. *Signal Process*., **157**, 107685. https://doi.org/10.1016/j.ymssp.2021.107685

Wan, H-P. and Ni, Y-Q. (2019), "Bayesian multi-task learning methodology for reconstruction of structural health monitoring data", *Struct*. *Health Monitor*., **18**(4), 1282-1309. https://doi.org/10.1177/1475921718794953

Wan, H-P. and Ni, Y-Q. (2018), "Bayesian modelling approach for forecast of structural stress response using structural health monitoring data", *J*. *Struct*. *Eng*., **144**(9). https://doi.org/10.1061/(ASCE)ST.1943-541X.0002085

Wang, J. and Shen, Y. (2019), "An enhanced Lamb wave virtual time reversal technique for damage detection with transducer transfer function compensation", *Smart Mater*. *Struct*., **28**(8), 085017. https://doi.org/10.1088/1361-665X/ab1fc8

Wang, Q., Ma, S. and Yue, D. (2018a), "Identification of damage in composite structures using Gaussian mixture model-processed Lamb waves", *Smart Mater*. *Struct*, **27**(4), 045007. https://doi.org/10.1088/1361-665X/aaaf96

Wang, W., Bao, Y., Zhou, W. and Li, H. (2018b), "Sparse representation for Lamb-wave-based damage detection using a dictionary algorithm", *Ultrasonics*, **87**, 48-58. https://doi.org/10.1016/j.ultras.2018.02.011

Wu, Z., Qing, X.P. and Chang, F-K. (2009), "Damage detection for composite laminate plates with a distributed hybrid PZT/FBG sensor network", *J*. *Intell*. *Mater*. *Syst*. *Struct*., **20**(9). https://doi.org/10.1177/1045389X08101632

Yeum, C.M., Sohn, H., Lim, H.J. and Ihn, J.B. (2014), "Reference free delamination detection using Lamb waves", *Struct*. *Control Health Monitor*., **21**(5), 675-684. https://doi.org/10.1002/stc.1594

Zeng, L., Lin, J. and Huang, L. (2017), "A modified Lamb wave time-reversal method for health monitoring of composite structures", *Sensors*, **17**(5), 955. https://doi.org/10.3390/s17050955

Zheng, Y., Liu, K., Wu, Z., Gao, D., Gorgin, R., Ma, S. and Lei, Z. (2019), "Lamb waves and electro-mechanical impedance based damage detection using a mobile PZT transducer set", *Ultrasonics*, **92**, 13-20. https://doi.org/10.1016/j.ultras.2018.06.008

Zhou, K., Zheng, Y., Zhang, J., Xu, X., Ma, S. and Wu, Z. (2019), "A reconstruction-based mode separation method of Lamb wave for damage detection in plate structures", *Smart Mater*. *Struct*., **28**(3), 035033. https://doi.org/10.1088/1361-665X/ab0299

Zhu, R., Huang, G.L. and Yuan, F.G. (2013), "Fast damage imaging using the time-reversal technique in the frequency wavenumber domain", *Smart Mater*. *Struct*., **22**(7), 075028. https://doi.org/10.1088/0964-1726/22/7/075028.

BS